Single-molecule imaging reveals the role of membrane-binding motif and C-terminal domain of RNase E in its localization and diffusion in *Escherichia coli*

Laura Troyer[1,6], Yu-Huan Wang[1,6], Shobhna[2,3], Seunghyeon Kim[1], Jeechul Woo[4], Emad Tajkhorshid[2,3,5*], and Sangjin Kim[1,5*]

[1]Department of Physics, University of Illinois at Urbana-Champaign, Urbana, IL, USA
[2]Theoretical and Computational Biophysics Group, NIH Center for Macromolecular Modeling and Visualization, Beckman Institute for Advanced Science and Technology, University of Illinois at Urbana-Champaign, Urbana, IL, USA
[3]Department of Biochemistry, University of Illinois at Urbana- Champaign, Urbana, IL, USA
[4]Moduli Technologies, LLC, Springfield, IL, USA
[5]Center for Biophysics and Quantitative Biology, University of Illinois Urbana–Champaign, Urbana, IL, USA
[6]These authors contributed equally.
*Correspondence: emad@illinois.edu, sangjin@illinois.edu

ABSTRACT

In *Escherichia coli*, RNase E is the key enzyme for RNA processing and mRNA degradation. Despite the conserved function across bacteria, the domain composition of RNase E varies significantly among species, possibly affecting the enzyme's subcellular localization, mobility, and function. In this work, we used super-resolution microscopy to find that 93% of RNase E is localized to the membrane in *E. coli* and exhibits slow diffusion comparable to polysomes diffusing in the cytoplasm. By replacing the native amphipathic membrane targeting sequence (MTS) with a transmembrane motif, we discovered that the MTS results in slower diffusion and stronger membrane binding than a transmembrane motif. Additionally, the evolutionarily divergent C-terminal domain (CTD) was shown to grant slow diffusion of RNase E but to weaken its membrane binding. By analyzing how membrane localization and diffusion of RNase E affect mRNA degradation rates *in vivo*, we provide new insights into RNase E's role in the spatiotemporal organization of RNA processes in bacterial cells.

INTRODUCTION

RNase E is the main endoribonuclease in *Escherichia coli*, known for its role in RNA processing and mRNA degradation[1-3]. It is an essential protein[4,5], and homolog proteins are found across many bacterial species[6-8]. The essentiality stems from the N-terminal domain (NTD) or the catalytic domain[9]. The NTD is followed by a membrane targeting sequence (MTS) and the C-terminal domain (CTD) or macromolecular interaction domain[2], where RhlB (a DEAD-box RNA helicase), PNPase (a 3'→5' exonuclease), and enolase (a glycolytic enzyme) bind to form the RNA degradosome complex[6]. The MTS forms an amphipathic α helix, responsible for the localization of RNase E in the inner membrane[10,11]. Interestingly, the membrane localization of RNase E and the presence of CTD are not essential in *E. coli* nor are conserved across bacterial species, in contrast to the broad conservation of NTD across bacteria as well as chloroplast[7,12,13]. This raises a question about the role of membrane localization and CTD in the *in vivo* function of RNase E.

E. coli strains with cytoplasmic RNase E (due to the removal of MTS) are viable although they grow slower than the wild-type (WT) cells[10,14]. *In vitro* studies showed that membrane binding of RNase E does not necessarily increase its enzymatic rates[10,14]. However, membrane localization is likely important for gene regulation *in vivo* because RNase E becomes sequestered from the cytoplasmic pool of mRNAs, giving mRNAs time for translation. This idea is supported by our recent observation that the membrane-bound RNase E limits the degradation of nascent mRNAs while cytoplasmic RNase E (ΔMTS) can degrade nascent mRNAs during transcription[15]. We found that transcripts encoding membrane proteins can be an exception to this rule, in that they can experience co-transcriptional degradation assisted by transertion effect[15]. These findings agree with results from a genome-wide study, indicating that the membrane localization of RNase E (but not the cytoplasmic localization of RNase E) allows for differential regulation of mRNA stability for genes encoding cytoplasmic proteins versus inner membrane proteins in *E. coli*[16].

Previous studies have reported evidence that *E. coli* RNase E can localize in the cytoplasm—for example, when cells were grown anaerobically[17] or when membrane fluidity was reduced by changes in lipid composition[18]. These findings imply that RNase

E can dissociate from the membrane; however, the origin of weak membrane binding remains unknown.

Across bacteria, several species within α-proteobacteria have cytoplasmic RNase E[19] while other species have membrane-bound RNase E. Among these, *B. subtilis* RNase Y (a functional homolog of RNase E) associates with the membrane via a transmembrane motif[20], instead of an amphipathic motif used by *E. coli* and other γ-proteobacteria[7]. Considering different types of membrane-binding motifs that evolution has introduced, *E. coli* RNase E may possibly be engineered with a transmembrane motif. Such a mutant will serve as a useful model for investigating the impact of membrane-binding motifs on the localization, diffusion, and activity of RNase E.

Lastly, the CTD of *E. coli* RNase E is a natively unstructured region[21] that has been shown to contribute to the enzymatic activity happening at the NTD[15,22-24]. We recently showed that this is likely due to an internal allosteric effect within RNase E, instead of the roles played by additional factors bound at the CTD, such as RhlB and PNPase[15]. Interestingly, CTD is not conserved across bacteria[7], and its contribution to the structural stability and membrane binding affinity of RNase E remains unknown.

In this study, we quantified the membrane binding percentage (MB%) of RNase E in *E. coli* cells using single-molecule microscopy and investigated how its membrane association affects its diffusion as well as its function in mRNA degradation. We examined the effects of different membrane-binding motifs, including the original MTS and transmembrane segments derived from LacY, on the localization and diffusion of RNase E, in the presence and absence of CTD. Our work provides new insights into the spatial organization of RNase E in bacteria and highlights the importance of MTS and CTD in regulating the localization, diffusion, and function of RNase E. Our findings offer potential avenues for modulating RNase E's subcellular localization and diffusion dynamics and hence its activity, for various applications.

RESULTS

Membrane binding percentage (MB%) of RNase E

Fluorescence microscopy studies have shown that RNase E is localized to the membrane in *E. coli*[10,11,16], but the percentage of molecules bound to the membrane has not been

quantitatively examined in live cells. To analyze RNase E localization and dynamics at the single-molecule level, we fused RNase E with a photo-convertible fluorescent protein, mEos3.2[25] and imaged individual RNase E molecules over time in two dimensions (**Fig. 1A**). The location of fluorescent molecules was identified in each frame and linked to form tracks using the open-source software u-track[26] (**Fig. 1A**). The subcellular locations were also calculated relative to the cell boundaries identified from bright-field images using another open-source image analysis package Oufti[27] (**Fig 1B**). To combine data from many cells, molecular positions along the short and long axes of a cell were normalized to the cell width and cell length for xNorm and yNorm, respectively (**Fig. 1C**). Based on the yNorm, molecules in the cylindrical part of cells were selected, and their xNorm values were used to obtain an xNorm histogram. Hereinafter, we will focus on the xNorm histogram to compare the membrane enrichment of proteins.

The xNorm histogram of RNase E shows two peaks corresponding to each side edge of the membrane (**Fig. 1D** and **Fig. S1**), very similar to the xNorm histogram of LacY, obtained by imaging LacY-mEos3.2 using the same method. LacY is a membrane channel for lactose and is composed of 12 transmembrane segments[28]. It is expected to be inserted into the inner membrane during translation[29-31], such that all imaged LacY is expected to be localized in the inner membrane[32].

We further quantified the percentage of molecules bound to the membrane (membrane-binding percentage or MB%) from the xNorm histogram. To do this, we developed a mathematical model based on a 2D projection of molecules randomly distributed on the surface of or inside a cylinder. The model includes imaging effects that affect the shape of xNorm histograms: the localization error, limited focal depth of the quasi-TIRF illumination we used, and the location of the inner membrane relative to the cell boundary (**Fig. S2**). The model fitting was performed using the Markov-Chain Monte Carlo algorithm (MCMC). For validation, we applied the model to xNorm histograms of LacY and LacZ for complete membrane binding or complete cytoplasmic localization, respectively. The MB% of LacY was 99% with a 95% confidence interval of [96%, 100%], and LacZ showed MB% of 3.4% [0.2%, 7.3%] (**Fig. 1E-F, Fig. S3A**). Both MB% agree with the expectation for membrane and cytoplasmic proteins. For RNase E, we found

MB% of 93% [91%, 96%], suggesting that most of the RNase E molecules are localized in the inner membrane (**Fig. 1E**).

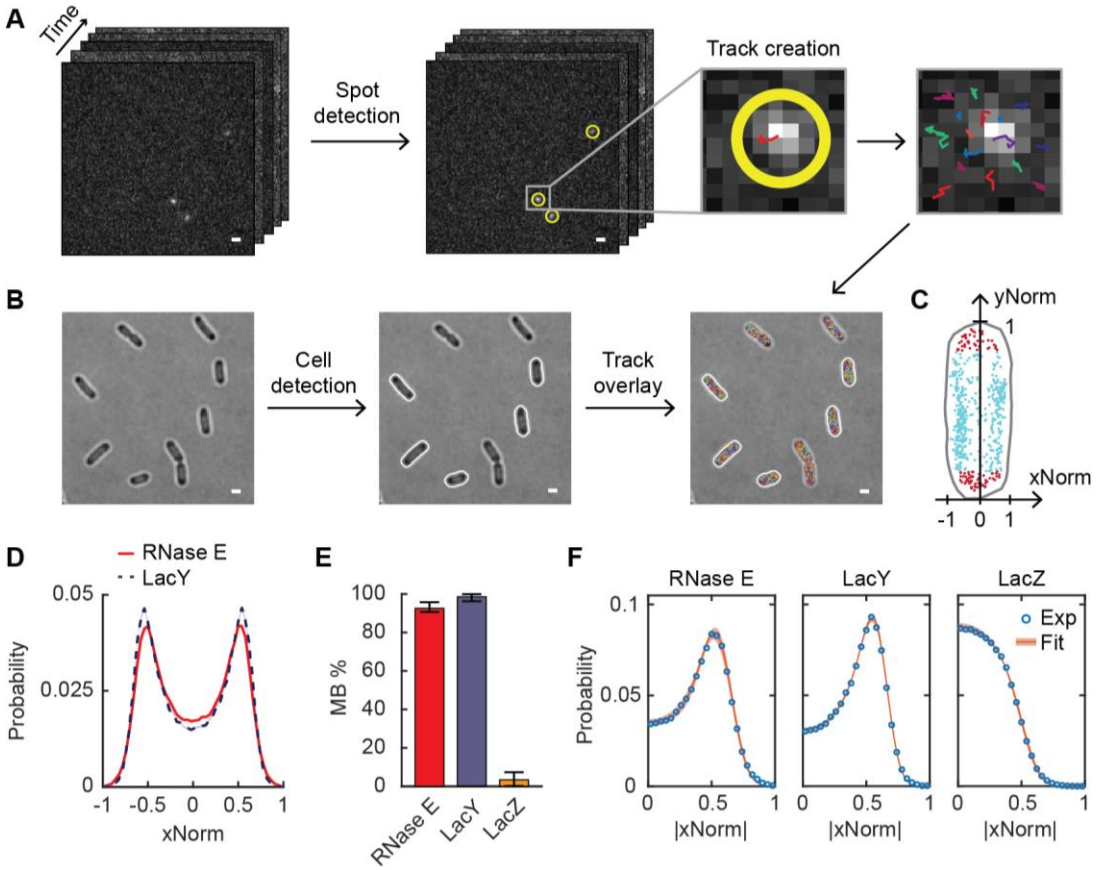

Figure 1: Analysis of single-molecule images for the subcellular localization and dynamics of proteins. (**A**) Single-molecule image analysis. Spots were detected in each frame (highlighted with yellow circles), and tracks were created across frames (different colors were chosen for different tracks). (**B**) Cell detection. Cell outlines were determined from bright-field images. Only non-dividing cells were analyzed (indicated by white outlines). (**C**) Normalized position of spots of RNase E along short (x) and long (y) axes of an example cell. Red spots are inside the cell endcaps, and cyan spots are in the cylindrical region of the cell. (**D**) xNorm histogram of RNase E and LacY. Only spots in the cylindrical region of cells (like cyan spots in **C**), over n = 143,000 spots, were included. The standard error of the mean (SEM) calculated from bootstrapping is displayed as a shaded area but is smaller than the line width (see **Fig. S1** for details). (**E**) The membrane binding percentage (MB%) of RNase E, LacY, and LacZ. Error bars are from the 95% confidence interval. (**F**) Histogram of absolute xNorm and model fitting of RNase E, LacY, and LacZ to determine MB%. Orange highlights indicate the range of xNorm expected based on the standard deviations in the parameter values estimated by MCMC. The white scale bars in panels **A**-**B** are 1 µm. See **Table S6** for data statistics.

Factors affecting slow diffusion of RNase E

The membrane localization of RNase E likely limits its interaction with mRNAs in the cytoplasm. We measured how fast RNase E moves in the membrane by analyzing the trajectories of individual RNase E-mEos3.2 imaged at 21.7 ms acquisition interval (**Fig. 1A**). We calculated the diffusion coefficient *D* by fitting the mean-squared displacement (MSD) of trajectories with MSD = $4D\tau + b$, where τ is lag time and *b* is a combination of dynamic and static localization error[33] (**Supplementary Information**). We obtained *D* of 0.0184 ± 0.0002 $\mu m^2/s$ (mean ± SEM) for RNase E (**Fig. 2A**). As a comparison, RNase E's *D* was larger than the low limit of *D* our microscope can measure from stationary, surface-immobilized mEos3.2, i.e. *D* = 0.0020 ± 0.0001 $\mu m^2/s$ (**Fig. S3A, Supplementary Discussion**). Also, RNase E's *D* was comparable to that of its RNA substrates, i.e. mRNAs bound with ribosomes, estimated to be *D* = 0.015 $\mu m^2/s$ based on the diffusion of ribosomal protein L1 (**Fig. S4C**). We investigated the origin of RNase E's slow mobility by testing the effect of (i) mRNA substrates, (ii) RNA degradosome components, and (iii) membrane attachment on the diffusion of RNase E.

To test the effect of mRNA substrates on the diffusion of RNase E, we treated cells with rifampicin, which blocks transcription initiation thus depleting cellular mRNAs. In rifampicin-treated cells, *D* of RNase E was 0.0270 ± 0.0003 $\mu m^2/s$, a 1.47-times increase from untreated cells (**Fig. 2B**). We note that LacY also exhibited a statistically significant increase in *D* in rifampicin-treated cells with a 1.25-times increase from untreated cells (**Fig. 2C**). Although this increase is relatively small, it was unexpected because LacY is not an RNA-binding protein. The increase in *D* of LacY in rifampicin-treated cells likely results from the depletion of mRNAs near the membrane (e.g., the mRNAs undergoing transertion), which could otherwise hinder the diffusion of membrane proteins[34,35].

The fact that RNase E exhibits less than a two-fold increase in *D* upon rifampicin treatment is surprising. In the case of the ribosome, the diffusion of its large subunit L1 protein was 7 times faster in rifampicin-treated cells (**Fig. 2D**), consistent with previous reports[36,37]. This big change can be explained by the fact that ribosomes form polysomes, such that the effective mass of L1 protein in non-treated cells would be 2 or more times larger than that in rifampicin-treated cells (where it remains as a free subunit). In the case of RNase E, it forms the RNA degradosome complex, whose mass can be from 450 kDa[6]

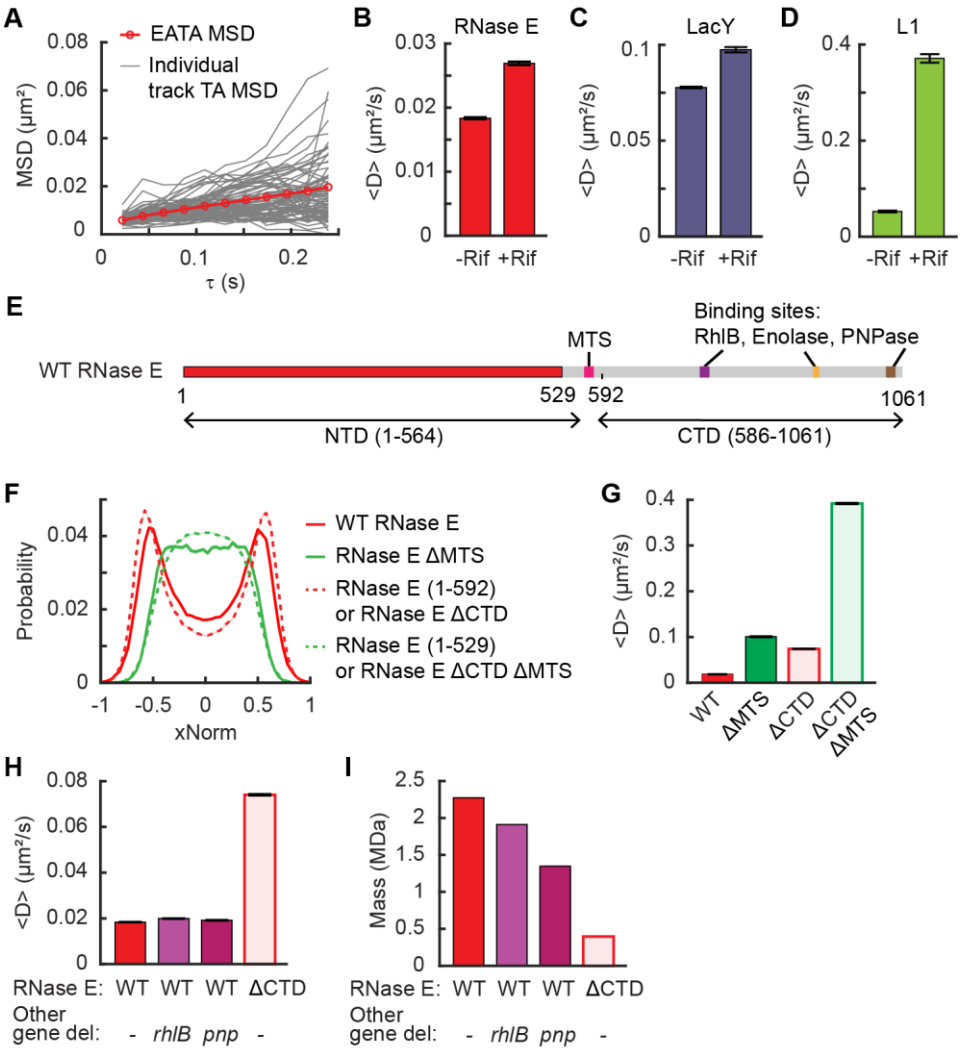

Figure 2: Effects of mRNA, MTS, and CTD on dynamics and localization of RNase E. (**A**) MSD versus time delay (τ) of RNase E. Ensemble-averaged time-averaged (EATA) MSD was calculated by averaging the time-averaged MSD of individual tracks. (**B-D**) Change in the mean diffusion coefficient of RNase E (**B**), LacY (**C**), and ribosome L1 protein (**D**) when cellular RNAs were depleted by rifampicin treatment. (**E**) Linear representation of RNase E monomer. Note that in this study we define CTD as the region following MTS. The numbers indicate amino acid residues. (**F**) xNorm histograms of various RNase E mutants. The SEM from bootstrapping is displayed but smaller than the line width. (**G**) Mean diffusion coefficients of various RNase E mutants, lacking MTS and/or CTD. (**H**) Mean diffusion coefficients of RNase E upon removal of different RNA degradosome components. (**I**) Expected mass of fully occupied RNA degradosome upon removal of different degradosome components. Error bars in panels **B-D** and **G-H** are the SEM. At least,1,100 tracks for diffusion data or 90,000 spots for xNorm data were used in the analysis. See **Table S6** for data statistics.

to 2.3 MDa depending on the partial or full occupancy of the canonically known component proteins (RhlB, PNPase, enolase)[2,38-41] (**Supplementary Discussion)**. In either case, the RNase E complex is smaller than the 70S ribosome of ~2.5 MDa[42]. If RNase E interacts with an mRNA with n ribosomes, the total mass of the RNA degradosome complex would increase by (n + 1) fold or more. Thus, a substantial increase in *D* of RNase E is expected upon mRNA depletion.

To explain the marginal increase in RNase E's diffusion upon rifampicin treatment, we considered two possibilities; it is possible that only a small percentage of RNase E interacts with mRNAs and/or RNase E interacts with mRNA very briefly, unlike ribosomes spending an order of 10-100 s in a polysome state for translation elongation[43]. When we increased the polysome pool of the cellular mRNA by treating cells with a translation elongation inhibitor chloramphenicol[44] or by overexpressing *lacZ* mRNA from a high-copy plasmid, *D* of RNase E remained unchanged from untreated cells (**Fig. S4D**). This result rules out the possibility that only a small percentage of RNase E interacts with mRNAs and weighs in favor of the scenario that RNase E interacts with mRNAs briefly.

Next, we investigated the effect of membrane association on the diffusion of RNase E by comparing *D* of the WT RNase E with a cytoplasmic RNase E mutant lacking the MTS segment. The WT RNase E and RNase E ΔMTS have a similar molecular mass since MTS is only 15 residues of 1000 residues in a monomer RNase E (**Fig. 2E** and **Fig. S5**). Therefore, the difference in *D* should be attributed to their subcellular localizations (**Fig. 2F**; membrane vs cytoplasm) instead of the mass. We found that the cytoplasmic RNase E diffuses ~5.5 times faster than the membrane-bound, WT RNase E (**Fig. 2G**). A similar increase (~5.3 times) was observed when we examined the CTD truncation mutants, membrane-bound RNase E (1-592) and cytoplasmic RNase E (1-529), which have similar mass but different localizations (**Fig. 2F-G**).

The CTD region is where the RNA degradosome proteins (enolase, RhlB, and PNPase) bind to create the large RNA degradosome complex (**Fig. 2E**). To test how these proteins affect the diffusion of RNase E, we measured the diffusion of RNase E in strains where *rhlB* or *pnp* was deleted. *D* increased 1.08 and 1.04 times for Δ*rhlB* and Δ*pnp*, respectively. The increase was very minute (especially for Δ*pnp*), considering that the mass of the RNA degradosome is expected to decrease by 15% and 40% for *rhlB*

and *pnp* deletions, respectively (**Fig. 2H-I**). This finding possibly suggests complex stoichiometry in the RNA degradosome (see Discussions). Despite this ambiguity, a significant 4.04 times increase in *D* was observed in RNase E ΔCTD, or RNase E (1-592), where the CTD of RNase E was deleted to eliminate interactions with all RNA degradosome components while keeping the membrane localization (**Fig. 2H**). In this mutant, the mass of the RNase E complex is expected to decrease to 396 kDa (**Fig. 2I**). Altogether, these results suggest that the slow diffusion of RNase E is largely affected by the membrane localization and the formation of the massive RNA degradosome and less by interaction with mRNA substrates, unlike other RNA-interacting proteins, such as ribosomes.

Diffusion and localization of MTS and transmembrane segments

Unlike RNase E in *E. coli*, RNase Y, a functional homolog of RNase E in *B. subtilis*, is localized to the membrane via a transmembrane domain. Any differences between a peripheral (like MTS of *E. coli*'s RNase E) and a transmembrane motif on membrane localization and mobility of RNase E, remain unclear. To address this question, we created RNase E mutants that contain a transmembrane domain in place of the MTS.

Before creating the mutants, we characterized individual short membrane-binding motifs by fusing them with mEos3.2. LacY in its native form has 12 transmembrane segments that are spatially arranged into two groups of 6 transmembrane segments[28]. We were able to express the first two transmembrane segments (LacY(1-73) or LacY2), the first six transmembrane segments (LacY(1-192) or LacY6), and the original LacY (LacY12) fused to mEos3.2 from the IPTG-inducible promoter on the chromosome. We then imaged their membrane localization and diffusivity (**Fig. 3A**). The MTS segment and LacY-derived transmembrane segments showed a strong membrane enrichment (**Fig. 3B**). In terms of diffusion, LacY2 and LacY6 diffused faster than the MTS segment (**Fig. 3C**). This is remarkable because their molecular masses (and thus size) are expected to be larger than that of MTS (**Fig. 3D**). The Saffman-Delbruck diffusion model states that the diffusion coefficient of membrane proteins decreases logarithmically as the radius of the embedded part increases given the same membrane environment[45]. Our data

suggest that the two types of membrane-binding motifs (MTS and LacY2) experience different membrane environments, possibly due to the way they interact with the lipids.

To further explore protein-membrane interactions, we conducted all-atom molecular dynamics simulations of MTS and LacY2 interacting with the *E. coli* membrane using the NAMD software[46] (**Fig. 3E**; see **Supplementary Information**). In the simulations, protein motion was calculated for 1 µs. Although the *D* values were larger than the experimental values (possibly due to the absence of mEos3.2 in the model), MTS again diffused slower than LacY2 (**Fig. 3F** and **Fig. S6A**). By calculating membrane-protein interaction energies, we found that MTS-membrane interaction is more stable than LacY2-membrane interaction (**Fig. S6B**). These results suggest that the diffusion of MTS, located on the surface of the membrane, is slower than that of LacY2 due to stronger interaction with lipid head groups.

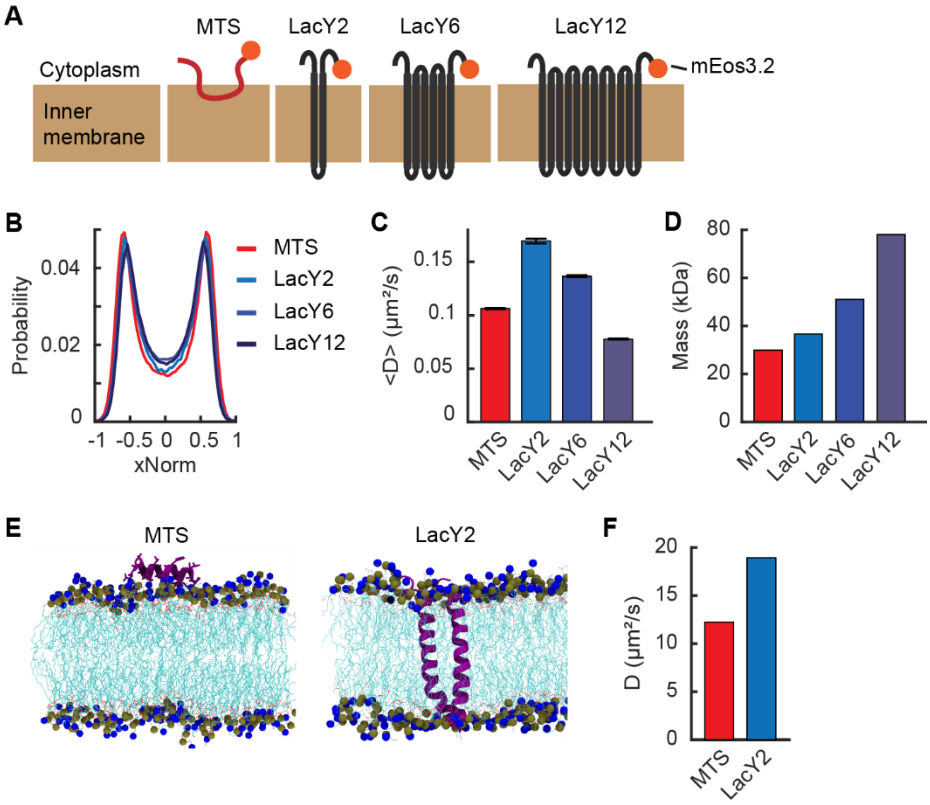

Figure 3: Localization and diffusion of membrane-binding motifs. (**A**) Cartoon schematic of the membrane-binding motifs used in this study (not to scale). The orange circles indicate mEos3.2 used for imaging. (**B**) xNorm histograms of membrane-binding motifs. The SEM from bootstrapping is displayed but smaller than the line width. Data are from at least 107,000 spots. (**C**) Mean diffusion coefficients of membrane-binding

motifs. Error bars are the SEM from at least 3,000 tracks. (**D**) Estimated mass of membrane-binding motifs based on the amino acid sequence including linkers and mEos3.2. (**E**) Snapshots from all-atom MD simulation of MTS and LacY2 in the *E. coli* membrane. The proteins are displayed in purple, and lipid tails are shown in cyan. Nitrogen and phosphorus atoms of the lipid head groups are represented in the van der Waals form in blue and grey, respectively. (**F**) Diffusion coefficients of MTS and LacY2 from the simulation. For panels **B** and **C**, see **Table S6** for data statistics.

RNase E mutants carrying a transmembrane motif

Since LacY2 and LacY6 showed a strong membrane enrichment similar to LacY12 (**Fig. 3B**), we replaced MTS in RNase E with LacY2, LacY6, and LacY12 in the presence or absence of CTD (**Fig. 4A-B** and **Fig. S5**). All the chimeric RNase E mutants were expressed from the native locus on the chromosome as the only copy of RNase E and had mEos3.2 fused at the C terminus for imaging. The strains did not show noticeable differences in growth rate compared to the WT strain (**Table S3**), suggesting that the RNase E mutants were functionally active.

xNorm histograms of ΔCTD mutants indicated membrane localization similar to LacY (**Fig. 4C**). However, mutants containing CTD showed noticeable cytoplasmic subpopulations when LacY2 and LacY6 were used in place of MTS (**Fig. 4D**). The mathematical model fitting of xNorm histograms suggested that MB% of RNase E-LacY2-CTD and RNase E-LacY6-CTD to be 69% [66%, 73%] and 86% [84%, 90%], respectively (**Fig. 4F**). We note that the non-perfect membrane localization was observed only in the mutants containing CTD and the same protein without CTD showed MB% of 100% (**Fig. 4E-F, Fig. S7A-B**). This observation suggests that CTD contributes to the unstable membrane binding of RNase E mutants. Such a difference between the presence and absence of CTD was not observed in the chimera based on LacY12 (**Fig. 4E-F**), possibly due to a stable membrane insertion of LacY12.

Membrane lipid composition is affected by the central metabolism[47] and hence, may be different when cells are grown in a different carbon source. To test the possibility that MB% of RNase E changes in different media (due to changes in the membrane property), we imaged RNase E from cells grown in M9 succinate (instead of M9 glycerol with casamino acids and thiamine, CAAT; see **Table S3** for growth rate difference). We found that MB% of RNase E-LacY2-CTD reduced even lower to 43% [41%, 46%] (**Fig. S7C**).

This large reduction contrasted with the small MB% change observed in WT RNase E (from 93% to 92%) and LacY2 (from 99.6% to 100%) when cells were grown in M9 succinate, suggesting that RNase E-LacY2-CTD may exhibit a broad MB% range across different growth conditions (**Fig. S7C-D**).

Next, we examined whether the diffusion coefficients of chimeric RNase E mutants differed based on the type of membrane motifs they had. For example, MTS diffused slower than LacY2, despite being smaller in size (**Fig. 3C-D**). From this, we expected the

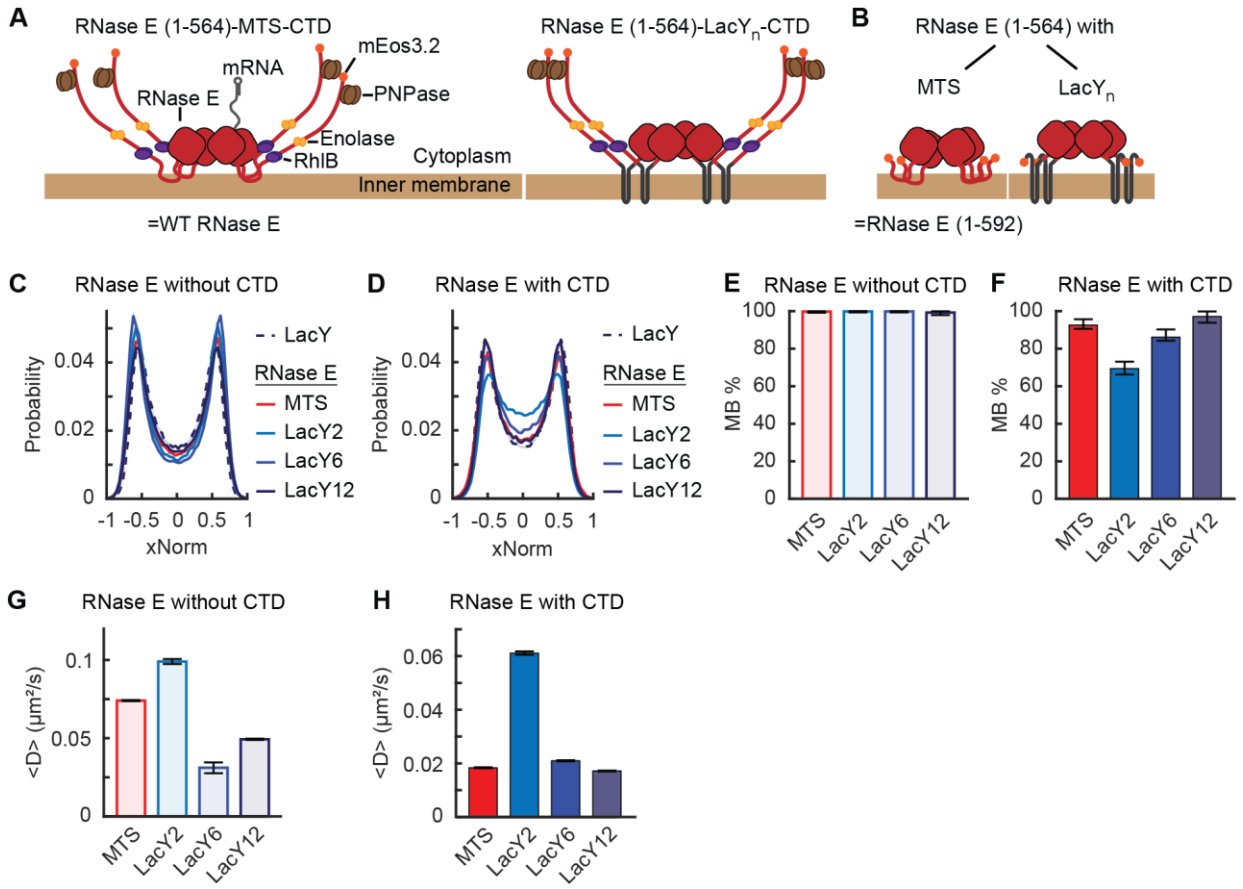

Figure 4: Localization and diffusion of chimeric RNase E with or without CTD. (**A-B**) Cartoon schematic of RNase E chimeric variants with CTD (**A**) and without CTD (**B**). They are not to scale. (**C-D**) xNorm histograms of chimeric RNase E localization compared with that of LacY. The SEM from bootstrapping is displayed but smaller than the line width. (**E-F**) MB% of chimeric RNase E mutants without CTD (**E**) or with CTD (**F**) with various membrane-binding motifs. Error bars are from a 95% confidence interval. (**G-H**) Mean diffusion coefficients of chimeric RNase E without CTD (**G**) or with CTD (**H**). Error bars are the SEM. Each data set contains at least 70,000 tracks for diffusion or 72,000 spots for xNorm (**Table S6**).

chimeric RNase E with LacY2 to diffuse faster than the RNase E with MTS. Indeed, in the absence of CTD, we found that LacY2-based RNase E diffuses 1.33 times faster than MTS-based RNase E (**Fig. 4G**). In the presence of CTD, LacY2 and LacY6-based RNase E diffused 3.33 and 1.14 times faster than the MTS-based RNase E counterpart (i.e. the WT RNase E). In this case (with CTD), the large increase in diffusion is also affected by the presence of cytoplasmic population (~31% for LacY2 and ~14% for LacY6; **Fig. 4H**) which diffuses faster than the membrane-bound population (possibly about 5 times faster, based on **Fig. 2G**). Taken together, our data suggest that transmembrane motifs can facilitate the diffusion of RNase E and allow for dissociation from the membrane in the presence of CTD.

Functional consequence of subcellular localization and diffusion of RNase E

To check the functional consequence of cytoplasmic localization of RNase E, we measured *lacZ* mRNA degradation in various RNase E mutants presented in this study. Recently, we developed an assay measuring co-transcriptional and post-transcriptional mRNA degradation rates of *lacZ* by inducing its transcription for only 75 s to capture the degradation of nascent mRNA[15]. We found that the rate of co-transcriptional degradation (k_{d1}) of *lacZ* mRNA is about 10 times slower than that of post-transcriptional degradation (k_{d2}) in WT cells. We found that k_{d1} increases about 3 fold in cells expressing RNase E ΔMTS, suggesting that cytoplasmic RNase E can freely diffuse and degrade nascent mRNAs in the cytoplasm, in contrast to the membrane-bound RNase E[15]. This result indicates that the chimeric RNase E that showed cytoplasmic subpopulation (**Fig. 4F**) may exhibit larger k_{d1} than other RNase E variants.

We repeated this assay in a strain expressing the WT RNase E fused with mEos3.2. Note that this strain is different from the one we used for imaging because a monocistronic *lacZ* gene is needed to aid data interpretation[15]. The relative abundances of 5' *lacZ* mRNA (Z5) before 3' *lacZ* mRNA (Z3) level increases (between ~100 and 210 s) were constant, confirming negligible co-transcriptional degradation of *lacZ* mRNA[15] (**Fig. 5A**). However, when we examined *lacZ* mRNA degradation in cells expressing RNase E-LacY2-CTD (69 MB%), the Z5 levels at the same time points exhibited a downward trend (**Fig. 5B**). Its k_{d1} was larger than any other RNase E mutants and close to what was observed in RNase E

ΔMTS[15] (**Fig. 5C**). RNase E-LacY6-CTD also showed some cytoplasmic population (86 MB%) but did not exhibit a significant increase in k_{d1} (**Fig. 5C**). The result from RNase E-LacY2-CTD suggests that the cytoplasmic subpopulation of RNase E is functional and may affect the degradation pattern of mRNAs globally.

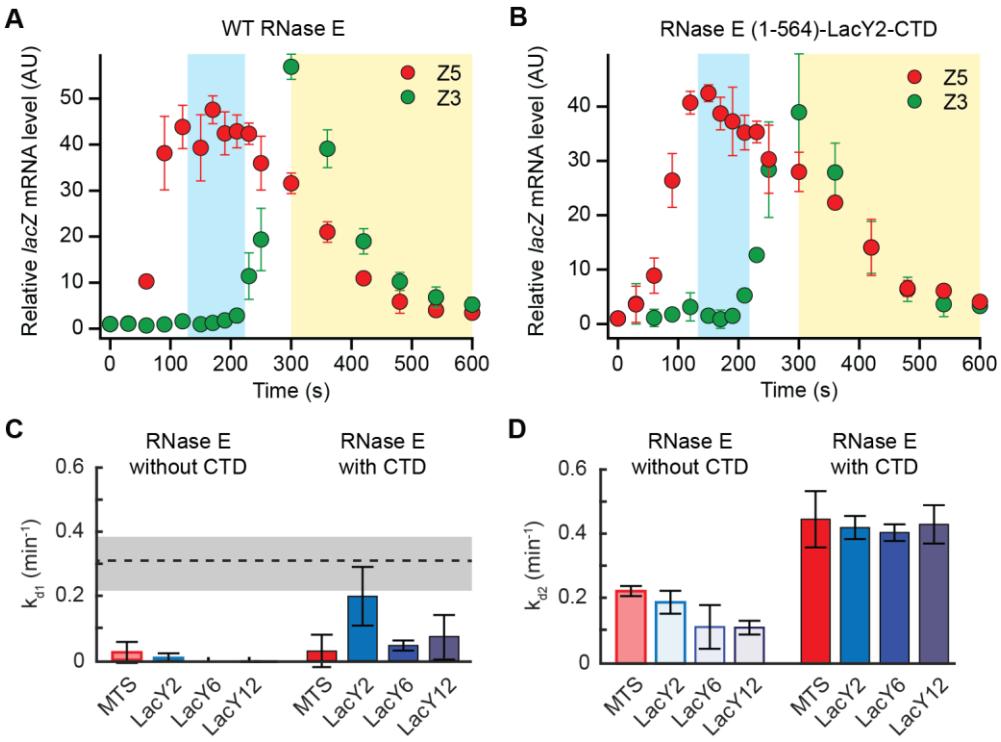

Figure 5: *lacZ* mRNA degradation rates in chimeric RNase E strains. (**A-B**) *lacZ* mRNA levels in RNase E with MTS and CTD or WT RNase E (**A**, strain SK595) and in RNase E-LacY2-CTD (**B**, strain SK505) when *lacZ* transcription was induced with 0.2 mM IPTG at t = 0 s and re-repressed with 500 mM glucose at t = 75 s. Blue and yellow regions indicate where k_{d1} and k_{d2} were measured by the exponential fitting of *lacZ* 5' mRNA (Z5) in individual replicates. (**C-D**) Co-transcriptional and post-transcriptional *lacZ* mRNA degradation rates, k_{d1} (**C**) and k_{d2} (**D**), respectively, in various strains of chimeric RNase E with different membrane-binding motifs, either ΔCTD (light bars) or with CTD (solid bars). The dotted line indicates the k_{d1} value of cytoplasmic RNase E ΔMTS (strain SK339)[15]. RNase E ΔCTD based on LacY6 and LacY12 showed zero k_{d1}. In all panels, error bars are the standard deviations from 3 biological replicates.

In terms of the post-transcriptional mRNA degradation rate (k_{d2}), we tested if the slow diffusion of RNase E in the membrane affects k_{d2}. In the presence of CTD, k_{d2} did not vary much among different membrane motifs (MTS and LacY; **Fig. 5D**). For example, even though the LacY12 motif slows down the diffusion of RNase E, k_{d2} was similar to

that of WT RNase E (**Fig. 5D**). This might be due to differences in RNase E copy numbers. Specifically, the LacY12 version of RNase E might be more abundant than the WT version because RNase E expression level is affected by its ability to regulate its own transcript levels[48]. The higher expression level might compensate for the slow diffusion to give a similar k_{d2}. However, when we examined the over-expression of WT RNase E, we observed that k_{d1} and k_{d2} remained unaffected (**Fig. S8A**). These results suggest that k_{d2} is not limited by the copy number and diffusion of membrane-bound RNase E in the presence of CTD.

In the absence of CTD, k_{d2} was, in general, lower than those measured from RNase E variants including CTD (**Fig. 5D**), indicating the importance of CTD in RNase E's catalytic activity. Similar results have been reported earlier for RNase E based on MTS[15,22-24]. Among different membrane motifs for RNase E ΔCTD, we noticed that the LacY2 version, which diffuses faster than the MTS version (**Fig. 4G**), does not necessarily yield higher k_{d2} (**Fig. 5D**). Plus, LacY6 and LacY12 versions showed even lower k_{d2} than MTS-based RNase E ΔCTD. Overall, the slow k_{d2} coming from the absence of CTD could not be rescued by faster diffusion of RNase E, but it can be worsened by the large and slow membrane motifs. The presence of CTD appears to buffer the effect of membrane motifs on the catalytic activity of RNase E (k_{d2}).

DISCUSSION

Our study establishes the membrane enrichment and slow diffusion of RNase E in *E. coli*. This supports the notion that sequestration of RNase E on the membrane confers the spatial and temporal separation between synthesis and decay of mRNAs[15]. Furthermore, the processing of rRNA[49-53] and tRNA[54,55] and small RNA-based gene regulations[56,57] mediated by RNase E likely take place on the membrane.

For the WT RNase E, our analysis showed MB% of 93%, close to 91% observed using immunogold labeling and freeze-fracture method in a previous study[58]. Because the membrane localization of RNase E was shown to be affected by membrane lipid composition[18], we tested if the MB% of WT RNase E changes in different growth conditions. When cells were grown in M9 with succinate as a sole carbon source without CAAT, different from the media used in all our measurements (M9 glycerol with CAAT),

the MTS segment exhibited MB% reduction from 100% to 83% while the LacY2 segment maintained ~100% (**Fig. S3E, S3G, S6D**), suggesting that MTS can lose membrane binding affinity in this condition. This result may be consistent with the fact that amphipathic motifs tend to have a weaker association with the membrane than transmembrane motifs due to peripheral interaction with the membrane[59]. For example, an amphipathic motif within MinD was observed to be completely cytoplasmic when the motif alone was expressed with a GFP fusion in *E. coli*[60]. MinD becomes a membrane protein as a dimer, suggesting that the dimer formation is needed for strong membrane association[60]. Similarly, the nature of tetramer formation may ensure membrane localization of RNase E when a single MTS exhibits weak membrane association. The MB% of WT RNase E was marginally affected by the growth media (**Fig. S3F-G**).

While individual transmembrane motifs exhibited stronger membrane association than amphipathic motif MTS, we found LacY2-based RNase E can lose membrane binding affinity, unlike MTS-based RNase E. This was observed only in the presence of the CTD of RNase E, suggesting that in addition to the membrane binding motif, the CTD also contributes to the membrane binding affinity. This idea is also supported by MB% results of 93% for WT RNase E (containing CTD) vs 100% for its ΔCTD version, RNase E (1-592). Similarly, the chimeric RNase E with LacY6 and CTD showed MB% of 86% while its ΔCTD version showed 100% (**Fig 4E-F**). Functionally, our mRNA degradation assay supported the idea that the CTD might have an allosteric effect on the NTD[24], affecting mRNA degradation rates. This was true regardless of the subcellular localization of RNase E: in the membrane, RNase E (1-592) showed lower k_{d2} than WT RNase E, and in the cytoplasm, RNase E (1-529) showed lower k_{d2} than RNase E ΔMTS[15]. Future analysis of the full RNase E structure and conformational dynamics would help address remaining questions on the role of CTD on MB% and the function of RNase E.

D of RNase E we measured in *E. coli* (0.0183 ± 0.0002 $\mu m^2/s$) is comparable to those measured in other bacterial species. For example, in *Caulobacter crescentus*, *D* of its cytoplasmic RNase E was shown to be about 0.03 $\mu m^2/s$[61]. The diffusion of RNase Y in *B. subtilis* was found in either a slow (0.031 $\mu m^2/s$) or fast (0.3 $\mu m^2/s$) state[62]. The authors showed that the slow population represents RNase Y binding to mRNA and/or the putative RNA degradosome while the fast population is freely diffusing RNase Y. We note

that our data do not show two distinct diffusion states for RNase E in *E. coli* (**Fig. S4B**), possibly suggesting stable formation of RNA degradosome complexes in *E. coli*, in contrast to the dynamic formation observed in *B. subtilis*.

Diffusion is affected by the size of the particle in a given medium[45], and it has been used to identify different size forms of a protein, due to biochemical interactions or complex formation[36,63]. Related, the diffusion of RNase E in Δ*rhlB* and Δ*pnp* backgrounds can be used to understand the stoichiometry of the RNA degradosome complex. We observed that the WT RNase E (and thus RNA degradosome) in Δ*rhlB* diffuses faster than that in Δ*pnp* strain. This result is inconsistent with the expectation that the size of RNA degradosome should decrease more by the absence of PNPase than that of RhlB. This expectation assumes that all binding sites for RhlB and PNPase in RNase E are occupied. However, it has been proposed that a PNPase (trimer) may interact with more than one RNase E monomer[2,41]. It indicates that the stoichiometry between PNPase and RNase E might be lower than expected, yielding a smaller mass reduction in the RNA degradosome when PNPase is absent.

RNA substrates interacting with RNase E can also increase the effective mass of RNase E and lower its *D* value. However, when cellular mRNAs were depleted by rifampicin treatment, we found that RNase E diffusion increased less than that of other RNA-binding molecules related to transcription and translation. For example, the large and small ribosomal subunits[36,37,64], tRNA[65], and RNA polymerase[44] showed a large (about 10-20 fold) increase in *D* upon rifampicin treatment. Interestingly, Hfq, an RNA chaperon involved in small RNA regulation together with RNase E, showed a moderate increase (~2 fold) in *D* when RNA is depleted by rifampicin[66]. We note that our result is consistent with previous studies that examined the effect of rifampicin on RNase E diffusion in *E. coli*[11,67] as well as RNase E in *C. crescentus* and RNase Y in *B. subtilis*[62,68]. These findings likely imply that RNase E (and RNase Y) interacts with its substrate for a short time duration, different from other RNA-binding proteins related to transcription and translation.

Lastly, the slow diffusion of MTS in comparison to LacY2 and LacY6 suggests that MTS is not an efficient membrane-binding motif for diffusion in the membrane. While our molecular dynamics simulations demonstrated that it originates from stronger interaction

energy between protein and the membrane, whether this can be generalized to any other peripheral and integral membrane motifs remains to be tested. We speculate that this can be a general phenomenon as peripheral motifs interact with lipids orthogonally while integral membrane motifs interact with the lipids in parallel and can diffuse together with them. Diffusion of membrane-bound molecules contains information about protein-lipid contacts and membrane dynamics[69]. Future studies may help address the distinct diffusion dynamics of MTS and transmembrane motifs.

ACKNOWLEDGMENTS

We thank Drs. Mark Arbing, Agamemnon Carpousis, Johan Elf, and Christine Jacobs-Wagner for strains. We thank Maggie Liu, Kavya Vaidya, and Zach Wang for their contributions in the early phase of this work and the members of Kim lab for critical reading of the manuscript. This work was supported by the NSF Center for Physics of Living Cells (1430124), NSF Science and Technology Center for Quantitative Cell Biology (2243257), NIH (R35GM143203; R24GM145965), and Searle Scholars Program.

AUTHOR CONTRIBUTIONS

L.T. and S.K. designed the research; L.T. and Y.W. performed imaging and analysis; L.T. and Se.K. measured mRNA lifetimes; LT, Se.K., and S.K. performed genetics; L.T., Y.W., and J.W. developed data analysis methods; S. performed all-atom MD simulations under supervision of E.T.; L.T. and S.K. wrote the manuscript with input from all authors. S.K. supervised the study.

COMPETING INTERESTS

The authors declare no competing interests.

REFERENCES

1 Mudd, E. A., Krisch, H. M. & Higgins, C. F. RNase E, an endoribonuclease, has a general role in the chemical decay of Escherichia coli mRNA: evidence that rne and ams are the same genetic locus. *Molecular Microbiology* **4**, 2127-2135 (1990). https://doi.org/https://doi.org/10.1111/j.1365-2958.1990.tb00574.x

2 Mackie, G. A. RNase E: at the interface of bacterial RNA processing and decay. *Nature Reviews Microbiology* **11**, 45-57 (2013). https://doi.org/10.1038/nrmicro2930

3 Hui, M. P., Foley, P. L. & Belasco, J. G. Messenger RNA degradation in bacterial cells. *Annual Review of Genetics* **48**, 537-559 (2014). https://doi.org/https://doi.org/10.1146/annurev-genet-120213-092340

4 Apirion, D. & Lassar, A. B. A conditional lethal mutant of Escherichia coli which affects the processing of ribosomal RNA. *Journal of Biological Chemistry* **253**, 1738-1742 (1978). https://doi.org/https://doi.org/10.1016/S0021-9258(17)34927-X

5 Babitzke, P. & Kushner, S. R. The Ams (altered mRNA stability) protein and ribonuclease E are encoded by the same structural gene of Escherichia coli. *Proceedings of the National Academy of Sciences* **88**, 1-5 (1991). https://doi.org/doi:10.1073/pnas.88.1.1

6 Carpousis, A. J. The RNA degradosome of Escherichia coli: an mRNA-degrading machine assembled on RNase E. *Annual Review of Microbiology* **61**, 71-87 (2007). https://doi.org/https://doi.org/10.1146/annurev.micro.61.080706.093440

7 Aït-Bara, S. & Carpousis, A. J. RNA degradosomes in bacteria and chloroplasts: classification, distribution and evolution of RNase E homologs. *Molecular Microbiology* **97**, 1021-1135 (2015). https://doi.org/https://doi.org/10.1111/mmi.13095

8 Mardle, C. E. *et al.* A structural and biochemical comparison of ribonuclease E homologues from pathogenic bacteria highlights species-specific properties. *Scientific Reports* **9**, 7952 (2019). https://doi.org/10.1038/s41598-019-44385-y

9 Callaghan, A. J. *et al.* Structure of Escherichia coli RNase E catalytic domain and implications for RNA turnover. *Nature* **437**, 1187-1191 (2005). https://doi.org/10.1038/nature04084

10 Khemici, V., Poljak, L., Luisi, B. F. & Carpousis, A. J. The RNase E of Escherichia coli is a membrane-binding protein. *Mol Microbiol* **70**, 799-813 (2008). https://doi.org/10.1111/j.1365-2958.2008.06454.x

11 Strahl, H. *et al.* Membrane recognition and dynamics of the RNA degradosome. *PLOS Genetics* **11**, e1004961 (2015). https://doi.org/10.1371/journal.pgen.1004961

12 Kaberdin, V. R. *et al.* The endoribonucleolytic N-terminal half of Escherichia coli RNase E is evolutionarily conserved in Synechocystis sp. and other bacteria but not the C-terminal half, which is sufficient for degradosome assembly. *Proceedings of the National Academy of Sciences* **95**, 11637-11642 (1998). https://doi.org/doi:10.1073/pnas.95.20.11637

13 Lee, K. & Cohen, S. N. A Streptomyces coelicolor functional orthologue of Escherichia coli RNase E shows shuffling of catalytic and PNPase-binding domains. *Molecular Microbiology* **48**, 349-360 (2003). https://doi.org/https://doi.org/10.1046/j.1365-2958.2003.03435.x

14 Hadjeras, L. *et al.* Detachment of the RNA degradosome from the inner membrane of Escherichia coli results in a global slowdown of mRNA degradation, proteolysis of RNase E and increased turnover of ribosome-free

transcripts. *Molecular Microbiology* **111**, 1715-1731 (2019). https://doi.org/https://doi.org/10.1111/mmi.14248

15 Kim, S., Wang, Y.-H., Hassan, A. & Kim, S. Re-defining how mRNA degradation is coordinated with transcription and translation in bacteria. *bioRxiv*, 2024.2004.2018.588412 (2024). https://doi.org/10.1101/2024.04.18.588412

16 Moffitt, J. R., Pandey, S., Boettiger, A. N., Wang, S. & Zhuang, X. Spatial organization shapes the turnover of a bacterial transcriptome. *eLife* **5**, e13065 (2016). https://doi.org/10.7554/eLife.13065

17 Murashko, O. N. & Lin-Chao, S. Escherichia coli responds to environmental changes using enolasic degradosomes and stabilized DicF sRNA to alter cellular morphology. *Proceedings of the National Academy of Sciences* **114**, E8025-E8034 (2017). https://doi.org/doi:10.1073/pnas.1703731114

18 Gohrbandt, M. *et al.* Low membrane fluidity triggers lipid phase separation and protein segregation in living bacteria. *The EMBO Journal* **41**, e109800 (2022). https://doi.org/https://doi.org/10.15252/embj.2021109800

19 Al-Husini, N., Tomares, D. T., Bitar, O., Childers, W. S. & Schrader, J. M. α-Proteobacterial RNA degradosomes assemble liquid-liquid phase-separated RNP bodies. *Molecular Cell* **71**, 1027-1039.e1014 (2018). https://doi.org/https://doi.org/10.1016/j.molcel.2018.08.003

20 Lehnik-Habrink, M. *et al.* RNase Y in Bacillus subtilis: a natively disordered protein that is the functional equivalent of RNase E from Escherichia coli. *Journal of Bacteriology* **193**, 5431-5441 (2011). https://doi.org/doi:10.1128/jb.05500-11

21 Callaghan, A. J. *et al.* Studies of the RNA degradosome-organizing domain of the Escherichia coli ribonuclease RNase E. *Journal of Molecular Biology* **340**, 965-979 (2004). https://doi.org/https://doi.org/10.1016/j.jmb.2004.05.046

22 Lopez, P. J., Marchand, I., Joyce, S. A. & Dreyfus, M. The C-terminal half of RNase E, which organizes the Escherichia coli degradosome, participates in mRNA degradation but not rRNA processing in vivo. *Molecular Microbiology* **33**, 188-199 (1999). https://doi.org/https://doi.org/10.1046/j.1365-2958.1999.01465.x

23 Leroy, A., Vanzo, N. F., Sousa, S., Dreyfus, M. & Carpousis, A. J. Function in Escherichia coli of the non-catalytic part of RNase E: role in the degradation of ribosome-free mRNA. *Molecular Microbiology* **45**, 1231-1243 (2002). https://doi.org/https://doi.org/10.1046/j.1365-2958.2002.03104.x

24 Islam, M. S., Bandyra, K. J., Chao, Y., Vogel, J. & Luisi, B. F. Impact of pseudouridylation, substrate fold, and degradosome organization on the endonuclease activity of RNase E. *RNA* **27**, 1339-1352 (2021). https://doi.org/10.1261/rna.078840.121

25 Zhang, M. *et al.* Rational design of true monomeric and bright photoactivatable fluorescent proteins. *Nature Methods* **9**, 727-729 (2012). https://doi.org/10.1038/nmeth.2021

26 Jaqaman, K. *et al.* Robust single-particle tracking in live-cell time-lapse sequences. *Nature Methods* **5**, 695-702 (2008). https://doi.org/10.1038/nmeth.1237

27 Paintdakhi, A. *et al.* Oufti: an integrated software package for high-accuracy, high-throughput quantitative microscopy analysis. *Molecular Microbiology* **99**, 767-777 (2016). https://doi.org/https://doi.org/10.1111/mmi.13264

28 Abramson, J. *et al.* Structure and mechanism of the lactose permease of Escherichia coli. *Science* **301**, 610-615 (2003). https://doi.org/doi:10.1126/science.1088196

29 Ahrem, B., Hoffschulte, H. K. & Müller, M. In vitro membrane assembly of a polytopic, transmembrane protein results in an enzymatically active conformation. *J Cell Biol* **108**, 1637-1646 (1989). https://doi.org/10.1083/jcb.108.5.1637

30 Nagamori, S., Vázquez-Ibar, J. L., Weinglass, A. B. & Kaback, H. R. In vitro synthesis of lactose permease to probe the mechanism of membrane insertion and folding. *Journal of Biological Chemistry* **278**, 14820-14826 (2003). https://doi.org/https://doi.org/10.1074/jbc.M300332200

31 Stochaj, U. & Ehring, R. The N-terminal region of Escherichia coli lactose permease mediates membrane contact of the nascent polypeptide chain. *European Journal of Biochemistry* **163**, 653-658 (1987). https://doi.org/https://doi.org/10.1111/j.1432-1033.1987.tb10914.x

32 Volkov, I. L. *et al.* Spatiotemporal kinetics of the SRP pathway in live E. coli cells. *Proceedings of the National Academy of Sciences* **119**, e2204038119 (2022). https://doi.org/doi:10.1073/pnas.2204038119

33 Savin, T. & Doyle, P. S. Static and dynamic errors in particle tracking microrheology. *Biophys J* **88**, 623-638 (2005). https://doi.org/10.1529/biophysj.104.042457

34 Binenbaum, Z., Parola, A. H., Zaritsky, A. & Fishov, I. Transcription- and translation-dependent changes in membrane dynamics in bacteria: testing the transertion model for domain formation. *Molecular Microbiology* **32**, 1173-1182 (1999). https://doi.org/https://doi.org/10.1046/j.1365-2958.1999.01426.x

35 Matsumoto, K., Hara, H., Fishov, I., Mileykovskaya, E. & Norris, V. The membrane: transertion as an organizing principle in membrane heterogeneity. *Frontiers in Microbiology* **6** (2015). https://doi.org/10.3389/fmicb.2015.00572

36 Sanamrad, A. *et al.* Single-particle tracking reveals that free ribosomal subunits are not excluded from the Escherichia coli nucleoid. *Proceedings of the National Academy of Sciences* **111**, 11413-11418 (2014). https://doi.org/doi:10.1073/pnas.1411558111

37 Bakshi, S., Siryaporn, A., Goulian, M. & Weisshaar, J. C. Superresolution imaging of ribosomes and RNA polymerase in live Escherichia coli cells. *Molecular Microbiology* **85**, 21-38 (2012). https://doi.org/https://doi.org/10.1111/j.1365-2958.2012.08081.x

38 Chandran, V. & Luisi, B. F. Recognition of enolase in the Escherichia coli RNA degradosome. *Journal of Molecular Biology* **358**, 8-15 (2006). https://doi.org/https://doi.org/10.1016/j.jmb.2006.02.012

39 Chandran, V. *et al.* Recognition and cooperation between the ATP-dependent RNA helicase RhlB and ribonuclease RNase E. *Journal of Molecular Biology* **367**, 113-132 (2007). https://doi.org/https://doi.org/10.1016/j.jmb.2006.12.014

40 Nurmohamed, S., McKay, A. R., Robinson, C. V. & Luisi, B. F. Molecular recognition between Escherichia coli enolase and ribonuclease E. *Acta Crystallographica Section D* **66**, 1036-1040 (2010). https://doi.org/doi:10.1107/S0907444910030015

41 Nurmohamed, S., Vaidialingam, B., Callaghan, A. J. & Luisi, B. F. Crystal structure of Escherichia coli polynucleotide phosphorylase core bound to RNase E, RNA and manganese: implications for catalytic mechanism and RNA degradosome assembly. *Journal of Molecular Biology* **389**, 17-33 (2009). https://doi.org/https://doi.org/10.1016/j.jmb.2009.03.051

42 Stark, H. *et al.* The 70S Escherichia coli ribosome at 23 å resolution: fitting the ribosomal RNA. *Structure* **3**, 815-821 (1995). https://doi.org/https://doi.org/10.1016/S0969-2126(01)00216-7

43 Dai, X. *et al.* Reduction of translating ribosomes enables Escherichia coli to maintain elongation rates during slow growth. *Nature Microbiology* **2**, 16231 (2016). https://doi.org/10.1038/nmicrobiol.2016.231

44 Stracy, M. *et al.* Live-cell superresolution microscopy reveals the organization of RNA polymerase in the bacterial nucleoid. *Proceedings of the National Academy of Sciences* **112**, E4390-E4399 (2015). https://doi.org/doi:10.1073/pnas.1507592112

45 Saffman, P. G. & Delbrück, M. Brownian motion in biological membranes. *Proceedings of the National Academy of Sciences* **72**, 3111-3113 (1975). https://doi.org/doi:10.1073/pnas.72.8.3111

46 Phillips, J. C. *et al.* Scalable molecular dynamics with NAMD. *Journal of Computational Chemistry* **26**, 1781-1802 (2005). https://doi.org/https://doi.org/10.1002/jcc.20289

47 Parsons, J. B. & Rock, C. O. Bacterial lipids: Metabolism and membrane homeostasis. *Progress in Lipid Research* **52**, 249-276 (2013). https://doi.org/https://doi.org/10.1016/j.plipres.2013.02.002

48 Schuck, A., Diwa, A. & Belasco, J. G. RNase E autoregulates its synthesis in Escherichia coli by binding directly to a stem-loop in the rne 5′ untranslated region. *Molecular Microbiology* **72**, 470-478 (2009). https://doi.org/https://doi.org/10.1111/j.1365-2958.2009.06662.x

49 Apirion, D. Isolation, genetic mapping and some characterization of a mutation in Escherichia coli that affects the processing of ribonucleic acid. *Genetics* **90**, 659-671 (1978). https://doi.org/10.1093/genetics/90.4.659

50 Bessarab, D. A., Kaberdin, V. R., Wei, C.-L., Liou, G.-G. & Lin-Chao, S. RNA components of Escherichia coli degradosome: evidence for rRNA decay. *Proceedings of the National Academy of Sciences* **95**, 3157-3161 (1998). https://doi.org/doi:10.1073/pnas.95.6.3157

51 Ghora, B. K. & Apirion, D. Structural analysis and in vitro processing to p5 rRNA of a 9S RNA molecule isolated from an rne mutant of E. coli. *Cell* **15**, 1055-1066 (1978). https://doi.org/https://doi.org/10.1016/0092-8674(78)90289-1

52 Li, Z., Pandit, S. & Deutscher, M. P. RNase G (CafA protein) and RNase E are both required for the 5′ maturation of 16S ribosomal RNA. *The EMBO Journal* **18**, 2878-2885 (1999). https://doi.org/https://doi.org/10.1093/emboj/18.10.2878

53 Roy, M. K., Singh, B., Ray, B. K. & Apirion, D. Maturation of 5-S rRNA: ribonuclease E cleavages and their dependence on precursor sequences. *European Journal of Biochemistry* **131**, 119-127 (1983). https://doi.org/https://doi.org/10.1111/j.1432-1033.1983.tb07238.x

54 Li, Z. & Deutscher, M. P. RNase E plays an essential role in the maturation of Escherichia coli tRNA precursors. *RNA* **8**, 97-109 (2002).
55 Ow, M. C. & Kushner, S. R. Initiation of tRNA maturation by RNase E is essential for cell viability in E. coli. *Genes & Development* **16**, 1102-1115 (2002). https://doi.org/10.1101/gad.983502
56 Ikeda, Y., Yagi, M., Morita, T. & Aiba, H. Hfq binding at RhlB-recognition region of RNase E is crucial for the rapid degradation of target mRNAs mediated by sRNAs in Escherichia coli. *Molecular Microbiology* **79**, 419-432 (2011). https://doi.org/https://doi.org/10.1111/j.1365-2958.2010.07454.x
57 Reyer, M. A. *et al.* Kinetic modeling reveals additional regulation at co-transcriptional level by post-transcriptional sRNA regulators. *Cell Reports* **36**, 109764 (2021). https://doi.org/https://doi.org/10.1016/j.celrep.2021.109764
58 Liou, G.-G., Jane, W.-N., Cohen, S. N., Lin, N.-S. & Lin-Chao, S. RNA degradosomes exist in vivo in Escherichia coli as multicomponent complexes associated with the cytoplasmic membrane via the N-terminal region of ribonuclease E. *Proceedings of the National Academy of Sciences* **98**, 63-68 (2001). https://doi.org/doi:10.1073/pnas.98.1.63
59 Papanastasiou, M. *et al.* The Escherichia coli peripheral inner membrane proteome. *Molecular & Cellular Proteomics* **12**, 599-610 (2013). https://doi.org/10.1074/mcp.M112.024711
60 Szeto, T. H., Rowland, S. L., Habrukowich, C. L. & King, G. F. The MinD membrane targeting sequence is a transplantable lipid-binding helix. *Journal of Biological Chemistry* **278**, 40050-40056 (2003). https://doi.org/https://doi.org/10.1074/jbc.M306876200
61 Bayas, C. A. *et al.* Spatial organization and dynamics of RNase E and ribosomes in Caulobacter crescentus. *Proceedings of the National Academy of Sciences* **115**, E3712-E3721 (2018). https://doi.org/doi:10.1073/pnas.1721648115
62 Oviedo-Bocanegra, L. M., Hinrichs, R., Rotter, Daniel Andreas O., Dersch, S. & Graumann, P. L. Single molecule/particle tracking analysis program SMTracker 2.0 reveals different dynamics of proteins within the RNA degradosome complex in Bacillus subtilis. *Nucleic Acids Research* **49**, e112-e112 (2021). https://doi.org/10.1093/nar/gkab696
63 Kapanidis, A. N., Uphoff, S. & Stracy, M. Understanding protein mobility in bacteria by tracking single molecules. *Journal of Molecular Biology* **430**, 4443-4455 (2018). https://doi.org/https://doi.org/10.1016/j.jmb.2018.05.002
64 Gray, W. T. *et al.* Nucleoid size scaling and intracellular organization of translation across bacteria. *Cell* **177**, 1632-1648.e1620 (2019). https://doi.org/https://doi.org/10.1016/j.cell.2019.05.017
65 Volkov, I. L. *et al.* tRNA tracking for direct measurements of protein synthesis kinetics in live cells. *Nature Chemical Biology* **14**, 618-626 (2018). https://doi.org/10.1038/s41589-018-0063-y
66 Park, S. *et al.* Dynamic interactions between the RNA chaperone Hfq, small regulatory RNAs, and mRNAs in live bacterial cells. *eLife* **10**, e64207 (2021). https://doi.org/10.7554/eLife.64207
67 Hamouche, L., Poljak, L. & Carpousis, A. J. Polyribosome-dependent clustering of membrane-anchored RNA degradosomes to form sites of mRNA degradation

in Escherichia coli. *mBio* **12**, 10.1128/mbio.01932-01921 (2021). https://doi.org/doi:10.1128/mbio.01932-21

68 Hamouche, L. *et al.* Dynamic membrane localization of RNase Y in Bacillus subtilis. *mBio* **11**, 10.1128/mbio.03337-03319 (2020). https://doi.org/doi:10.1128/mbio.03337-19

69 Knight, J. D., Lerner, M. G., Marcano-Velázquez, J. G., Pastor, R. W. & Falke, Joseph J. Single molecule diffusion of membrane-bound proteins: window into lipid contacts and bilayer dynamics. *Biophysical Journal* **99**, 2879-2887 (2010). https://doi.org/https://doi.org/10.1016/j.bpj.2010.08.046